Sensing Properties of Vacancy and Pd-Doped Graphene Layer: A First-Principles Study

Yanjie Xu
Chongqing University of Technology
Jun'an Zhang
Chongqing University of Technology
Yunhua Lu (yunhualul@163.com)
Chongqing University of Technology
Qingwei Zhang
Chongqing University of Technology
Lei Li
Yangtze Normal University
Jiangling Tian
Chongqing University of Technology

Research Article

Keywords: SO2 molecule, Graphene, Vacancy defect, Pd dopant, sensor application

Posted Date: July 8th, 2021

DOI: https://doi.org/10.21203/rs.3.rs-656641/v1

Sensing properties of vacancy and Pd-doped graphene layer: A first-principles study

Yanjie Xu[1], Jun'an Zhang[1], Yunhua Lu[1*], Qingwei Zhang[1], Lei Li[2], Jiangling Tian[1]

[1] School of Artificial Intelligence, Chongqing University of Technology, Chongqing, 401135, China

[2] Key Laboratory of Extraordinary Bond Engineering and Advanced Materials Technology (EBEAM) of Chongqing, Yangtze Normal University, Chongqing, 408100, China

*Corresponding auther E-mail: yunhualu1@163.com (Y.Lu)

Abstract: In this paper, the effect of SO_2 adsorption on graphene (intrinsic, vacancy, and doped) is investigated for structural and electronic properties to exploit their potential applications as a gas sensor. The adsorption energy, charge transfer, magnetic moment, density of states, as well as band structure of the SO_2 molecule on the vacancy and doped graphene systems are thoroughly discussed. The most stable adsorption site for SO_2 on various graphene sheets is also identified and reported. It is found that SO_2 molecule is weakly adsorbed on intrinsic graphene (IG) with low adsorption energy. In contrast, vacancy defect and Pd doping significantly enhance the strength of interaction between SO_2 molecule and the modified substrates. The dramatic increase in adsorption energy and charge transfer of these systems are expected to induce significant changes in the electrical conductivity of the vacancy graphene (VG) and Pd-doped graphene (PdG) sheets. Furthermore, the results present the potential of Pd-doped vacancy graphene (Pd-VG) for molecular sensor application.

Key words: SO_2 molecule; Graphene; Vacancy defect; Pd dopant; sensor application

1. Introduction

As industrialization advances rapidly, combating air pollution has become a global challenge. Gas sensor plays an irreplaceable role in numerous applications, including environmental monitoring, agricultural production, medical diagnosis, and aerospace [1–3]. Its value derives from the capacity to detect gas molecules in the environment at low concentrations, especially for toxic and harmful gases. Sulfur dioxide (SO_2) is the most common, simple and irritating sulfur oxide. It is one of the major air pollutants

resulting primarily from the combustion of coal, oil and other sulfur-containing minerals [4]. SO_2 is readily soluble in water and has a powerful stimulating effect on the eyes and breathing organs. Furthermore, SO_2 is the major cause of acid rain, which causes severe environmental damage. Meanwhile, SO_2 is one of the main decay products of gaseous SF_6 gas decomposition [5]. To control environmental acidification and ensure better GIS insulation, detecting residual SO_2 gases has become a priority for environmental surveillance. In recent years, numerous types of gas sensors have been designed for this purpose to accurately monitor SO_2 concentration levels and lay the foundation for environmental governance [6–10].

Graphene has generated considerable interest in the field of gas detection due to its extraordinary structural and electronic properties, such as ultra-high specific surface area, high electron mobility, and low electrical noise [11, 12]. Certain graphene-based sensors depend on changes in conductivity of graphene sheets due to changes in localized carrier density caused by surface adsorption, which acts as an electron donor or acceptor [13–15]. Compared to other nanoscale gas sensors, graphene is more appropriate for highly sensitive marked chemical sensors because every exposed carbon atom can provide information from the surrounding environment [16]. However, many studies have revealed that pristine graphene with the sp^2-hybridized carbon is almost insensitive to most gas molecules due to the insert π-electron conjugation, which limits its application as gas sensors [17–19]. To overcome this limitation, researchers attempted to construct sensitive graphene substrates by fabricating defective or doped atoms. The results showed that the dopants and defects could enhance the adsorption

between graphene and gas molecules [20–22]. For example, Rezvan *et al.* have reported a low-cost and simple-to-fabricate methane (CH_4) sensor by using graphene decorated with silver (Ag) nanoparticles [23]. Especially, this gas sensor can exhibit a higher response with the CH_4 gas concentrations less than 2000 ppm. Moreover, due to its mechanical flexibility, durability and high gas response, this sensor exhibits far better efficiency than previously reported ones. Highly sensitive boron-doped few-layer graphene sensor (BFLGs) was synthesized recently and used successfully for the detection of ammonia (NH_3) [24]. The authors also demonstrated that the BFLGs shows higher response and faster recovery compared to the pristine graphene sensor. Another study was that Shukri *et al.* explored the adsorption of CO and NO on pristine, vacancy, and Pd-doped graphene for structural and electronic properties [25]. The findings show that Pd-doping and vacancy can significantly improve the adsorption capacity of the modified graphene substrate on target gas molecules. Many studies have demonstrated by theoretical analysis and experiments that graphene can be employed as a gas sensor with doping extraneous atoms, introducing defect structure, and applying an electric field to possess appropriate band gap [26–28]. Hence, doping and defects have opened up numerous graphene-based applications, such as electronics and detection, due to the distinct nature of each dopant and defects.

In this paper, chapter 1 simulates the sensing applications of different graphene sheets for SO_2 molecule from first principles, including intrinsic graphene (IG), vacancy graphene (VG), Pd-doped graphene (PdG) and Pd-doped vacancy graphene (Pd-VG). The adsorption models are carefully constructed to systematically address

several fundamental issues. Chapter 2 provides details of the calculation. Chapter 3 analyzes and examines the most favorable adsorption configurations, adsorption energy, charge transfer, density of states (DOS), partial density of states (PDOS), and band structures of the systems. Chapter 4 concentrates on conclusions.

2. Computational details

All the theoretical calculations in our work were performed with the first-principles method based on DFT by using the Vienna ab-initio simulation package (VASP) with projector augmented wave (PAW) potentials [29–32]. To treat electron exchange and correlation, we chose the Perdew-Burke-Ernzerhof (PBE)[33] formulation of the generalized gradient approximation (GGA), which yields the correct ground-state structure of the combined systems. Plane-Wave basis function was set with a kinetic cut-off energy of 550 eV. A Monkhorst-Pack meshes[34] with the size of 5 × 5 × 1 were employed to the sample bulk Brillouin zone for the electronic properties. The distance between adjacent graphene layers was kept as 20 Å, which avoids the interactions between periodic images. The ground-state atomic geometries were optimized by relaxing the force below 0.02 eV/Å and the convergence criteria for energy was set with the value of 1.0×10^{-5} eV/cell. Tetrahedron method with Blöchl corrections[35] was employed for the electronic structures and total energy of our models while the Gaussian smearing was for stress/force relaxations. In order to better describe the interactions between molecules, van der Waals (vdW) interactions are included describing by the DFT-D3 method of Grimme [36]. The adsorption energy, E_{ads}, is defined as

$$E_{ads} = E_{graphene} + E_{SO_2} - E_{tot} \quad (1)$$

where $E_{graphene}$, E_{SO_2}, and E_{tot} represent the energy of the substrate, SO_2 molecule and each adsorption system, respectively. Considering the different molecular orientations and adsorption sites, the most stable adsorption configuration with the lowest total energy and the highest adsorption energy was obtained by calculation.

3. Results and discussion

3.1 Properties of adsorption configurations

To ensure the precision and reliability of the calculation, we constructed a stable adsorption substrate and a model of SO_2 molecule. Firstly, the geometric structures of IG and VG were optimized, then the doping behaviour of Pd atoms on the two relaxed structures was studied separately. The top and side views of the optimized geometries and the detailed parameters are presented in **Fig. 1**.

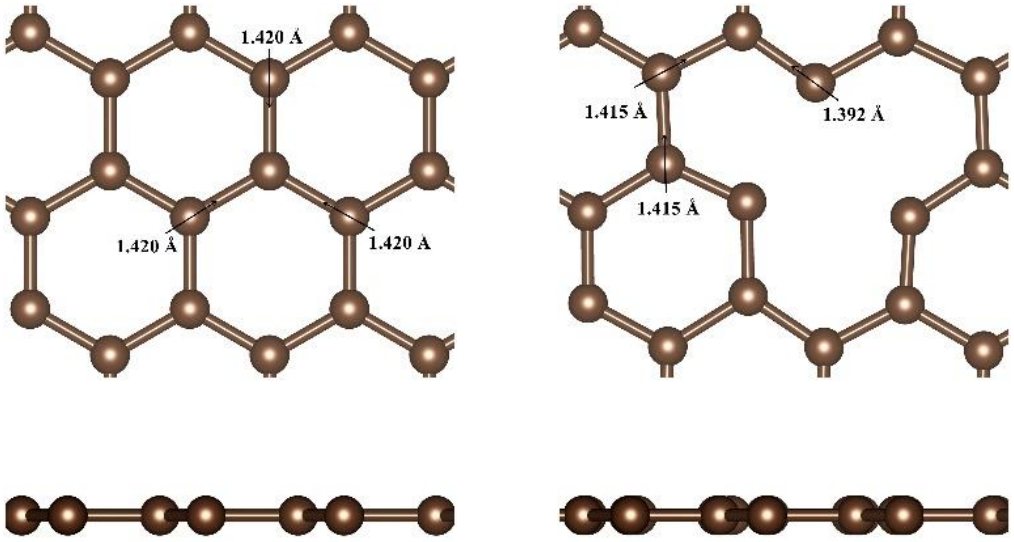

(a) IG (b) VG

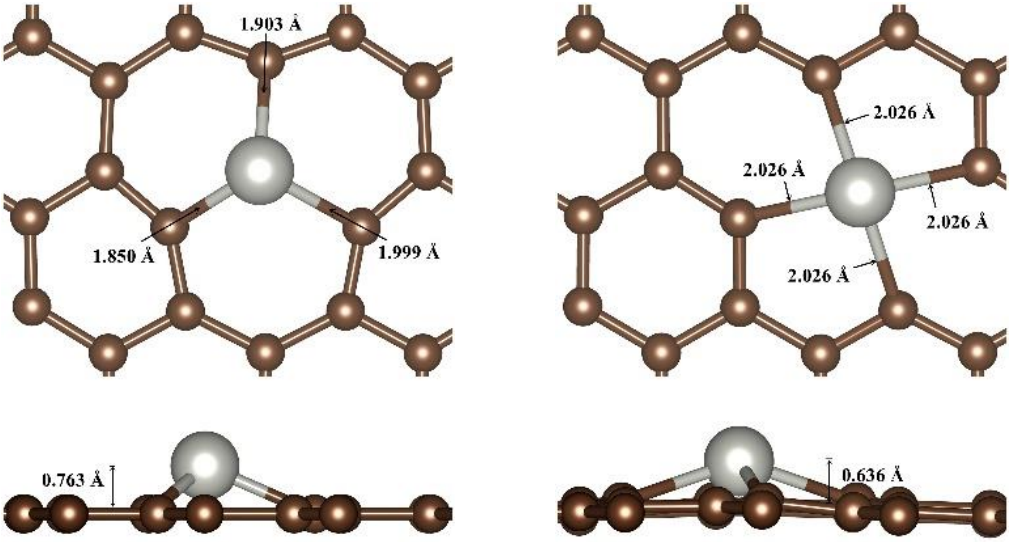

(c) PdG (d) Pd-VG

Fig. 1. The optimized geometry of graphene: (a) IG, (b) VG, (c) PdG, (d) Pd-VG. The brown and silver balls represent the carbon and palladium atoms, respectively.

The length of C-C bond on the optimized IG was 1.420 Å, corresponding to the experimental data, as shown in **Fig. 1(a)**. A central carbon atom is eliminated from IG to form VG, as shown in **Fig. 1(b)**. Unlike the IG structure, due to the strain caused by the loss of the central carbon atom, three carbon atoms break out of the graphene plane and the C-C bond near the vacancy is shortened in the range of 0.005 Å to 0.028 Å. Additionally, the PdG substrate was achieved by replacing the central C atom with Pd atom, as shown in **Fig. 1(c)**. It can be seen that the Pd atom protrudes from the graphene sheet with a protruding height of 0.763 Å. In addition, the doping site of the graphene sheet is deformed, and the Pd-C bond length is between 1.850 Å and 1.999 Å. The measurement parameters of the Pd-VG relaxation structure are illustrated in **Fig. 1(d)**. It has been observed that introducing Pd dopant in VG changes its geometry. Relative

to the VG, when a Pd atom is substituted for a carbon atom in VG, the Pd atom moves toward the defect center and form new Pd-C bonds with other hanging C atoms. Similarly, the Pd atom protrudes from the graphene sheet with a protrusion height of 0.636 Å. Pd atom prominence occurs because its radius is much larger than that of C atom. Meanwhile, Pd-VG shows the bond length between Pd to the nearest C atoms is 2.026 Å and the C-C bond length is 1.433 Å. The structural properties of Pd-VG change dramatically once the optimization has been carried out.

Next, we concentrated on comparing and analyzing the adsorption characteristics of SO_2 molecule on IG, VG, PdG and Pd-VG respectively. Taking the PdG layer as an example, four adsorption sites are hypothesized, traced as T_{Pd} (above the Pd atom), T_C(above the C atom), $B_{Pd\text{-}C}$(on the bridge site of Pd and C atoms), H_{6MR}(above the center of the six-membered ring, 6MR), each of which divided into two positions: S atom or O atom approaching graphene. After completing relaxation, the favorable configuration obtained from different initial adsorption points was compared to identify the most energetically stable one. The most stable configurations of SO_2 molecules on IG, VG, PdG, and Pd-VG are summarized in **Fig. 2**. The corresponding calculation details are summarized in **Table 1**.

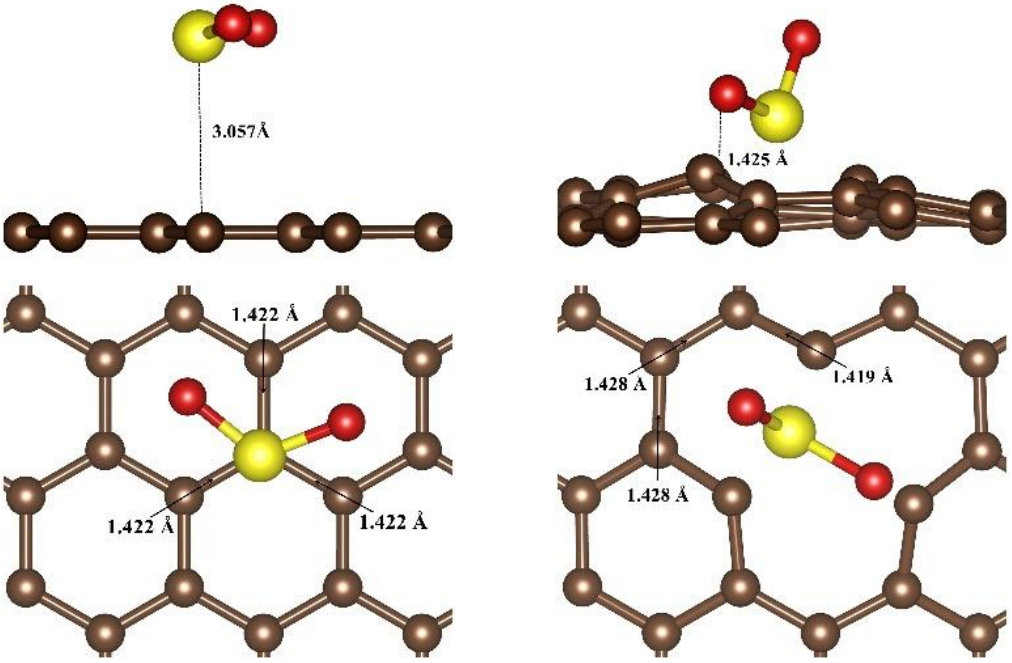

(a) SO_2-IG

(b) SO_2-VG

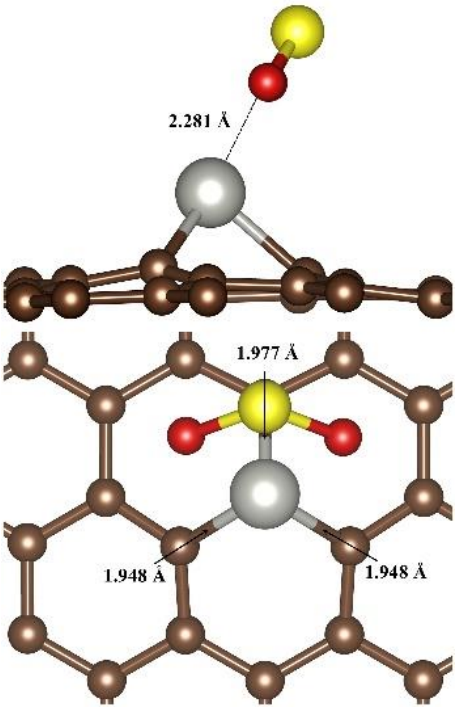

(c) SO_2-PdG

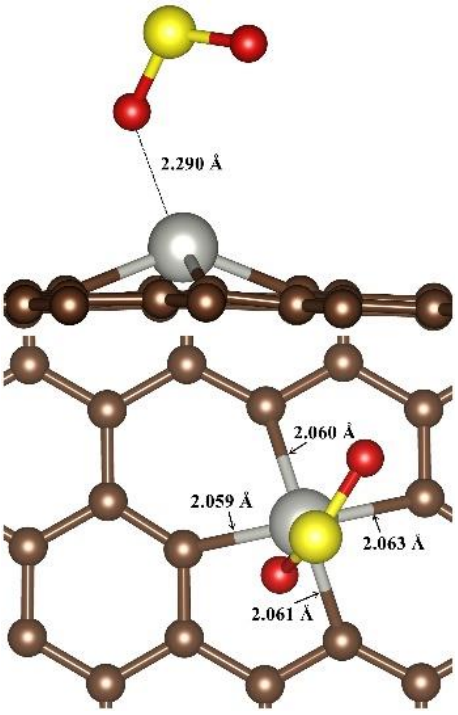

(d) SO_2-Pd-VG

Fig. 2. Optimized configurations for SO_2 adsorbed on: (a) IG, (b) VG, (c) PdG, (d) Pd-VG. Note that various configurations have been considered and we only present here the most stable configurations. Brown, silver, yellow and red balls represent the carbon,

palladium, sulfur and oxygen atoms, respectively.

Table 1

SO_2 adsorbed on IG, VG, PdG, and Pd-VG: adsorption energy (E_{ads}), adsorption length (l), bond length of SO_2 molecule after adsorption (d), band gap of the adsorption complex (E_g), charge transfer from the substrate to SO_2 molecule (ΔQ) and magnetic moment of the total system before adsorption (M) and after adsorption (M').

System	E_{ads}(eV)	l(Å)	d(Å)		E_g(eV)	$\Delta Q(e)$	M/M'(μB)
IG	0.295	3.057	1.453	1.453	0.02	0.105	0.000/0.000
VG	2.522	1.425	1.562	1.436	0.17	0.325	1.720/0.000
PdG	5.650	2.281	1.525	1.526	0.00	0.524	0.000/0.000
Pd-VG	0.734	2.392	1.456	1.463	0.40	0.276	0.000/0.000

Furthermore, the comparison of DOS curves of VG, PdG, and Pd-VG structures with those before modification is also examined, as shown in **Fig. 3**. Compared to the DOS of the IG, the Fermi level of PdG has obvious changes, and there is a peak crossing to the Fermi level of VG. In addition, it can be seen from **Fig. 3** that the band gap of PdG and Pd-VG structures are opened to varying degrees. Similar researches have confirmed that dopant or vacancy defect induced states close to the Fermi level would accelerate the charge transfer between the adsorption substrate and the adsorbent, causing changes in the adsorption mechanism of functionalized graphene systems [26, 37].

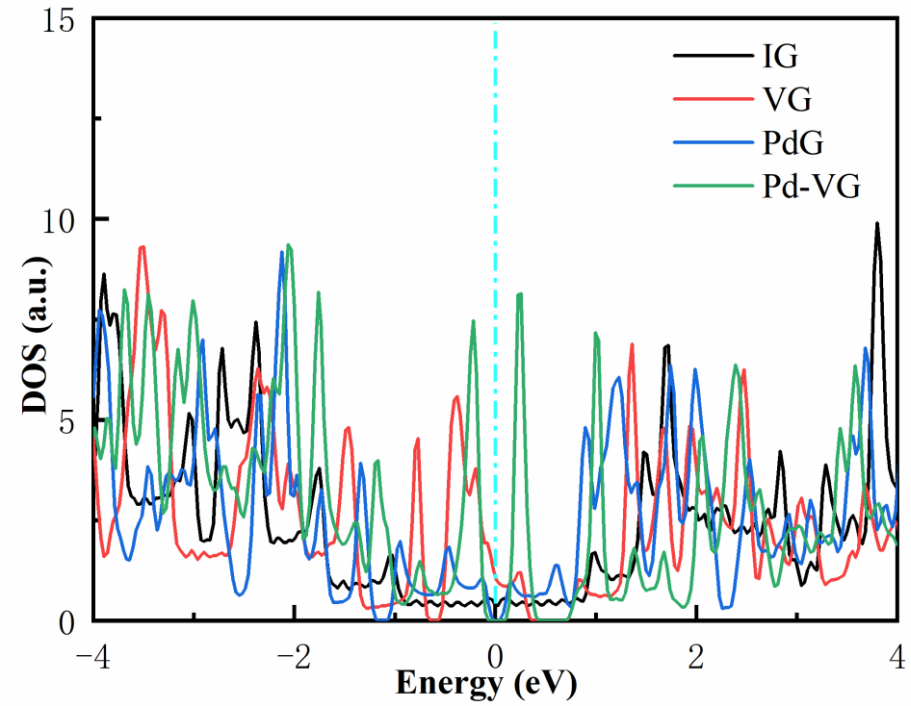

Fig. 3. DOS varies with energy curves for the IG, VG, PdG, and Pd-VG. The dotted line at zero indicates the Fermi level.

3.2 Adsorption performance of intrinsic graphene layer

We first discussed the adsorption behaviors of IG monolayer upon SO_2 molecule. Considering several possible initial positions (i.e. top site, bridge site, and hollow site) to obtain the best adsorption configuration. The optimal position is shown in **Fig. 2(a)** and the corresponding adsorption parameters are summarized in **Table 1**. After the adsorbing SO_2 molecule, the C-C bond in the interaction region is slightly elongated from 1.420 Å to 1.422 Å, and the S-O bond lengths of SO_2 are found to be 1.453 Å, which is also slightly elongated compared to the individual SO_2 molecule reported in the previous study [38]. From **Table 1**, the E_{ads} of SO_2 molecule on IG is 0.295 eV, and the adsorption distance is 3.057 Å. The lower E_{ads} and longer adsorption distance indicate typically physical adsorption. Bader charge analysis showed that 0.105e charge

was transferred from IG to SO_2 molecule, revealing that the SO_2 molecule acted as an acceptor in the adsorption phase.

To demonstrate the response of the SO_2 molecule to the electronic properties of IG layer, the total density of the polarized spin states of IG without and with adsorption of SO_2 has been calculated, as shown in **Fig. 4(a)**. It can be inferred that there is no spin polarization before and after IG adsorption, and the contribution of SO_2 molecule in the valence band is mainly between -4 eV and -3 eV, and in the conduction band around 0.5 eV. The DOS at Fermi level has no distinct change and the change in conductivity and magnetism is hardly noticeable. As shown in **Fig. 4(b)**, there is no hybridization between S-3p and O-2p orbitals of SO_2 molecule and C-2p orbitals around the Fermi level. The band structures of the adsorption system (before and after SO_2 adsorption) was calculated. It was observed that the band gap of IG layer was zero (see **Fig. 4(c)**), while a small band gap (E_g) about 0.02 eV, appeared after the adsorption of SO_2 molecule (see **Fig. 4(d)**). All calculated results indicate that IG is unsuitable for detecting SO_2 molecules.

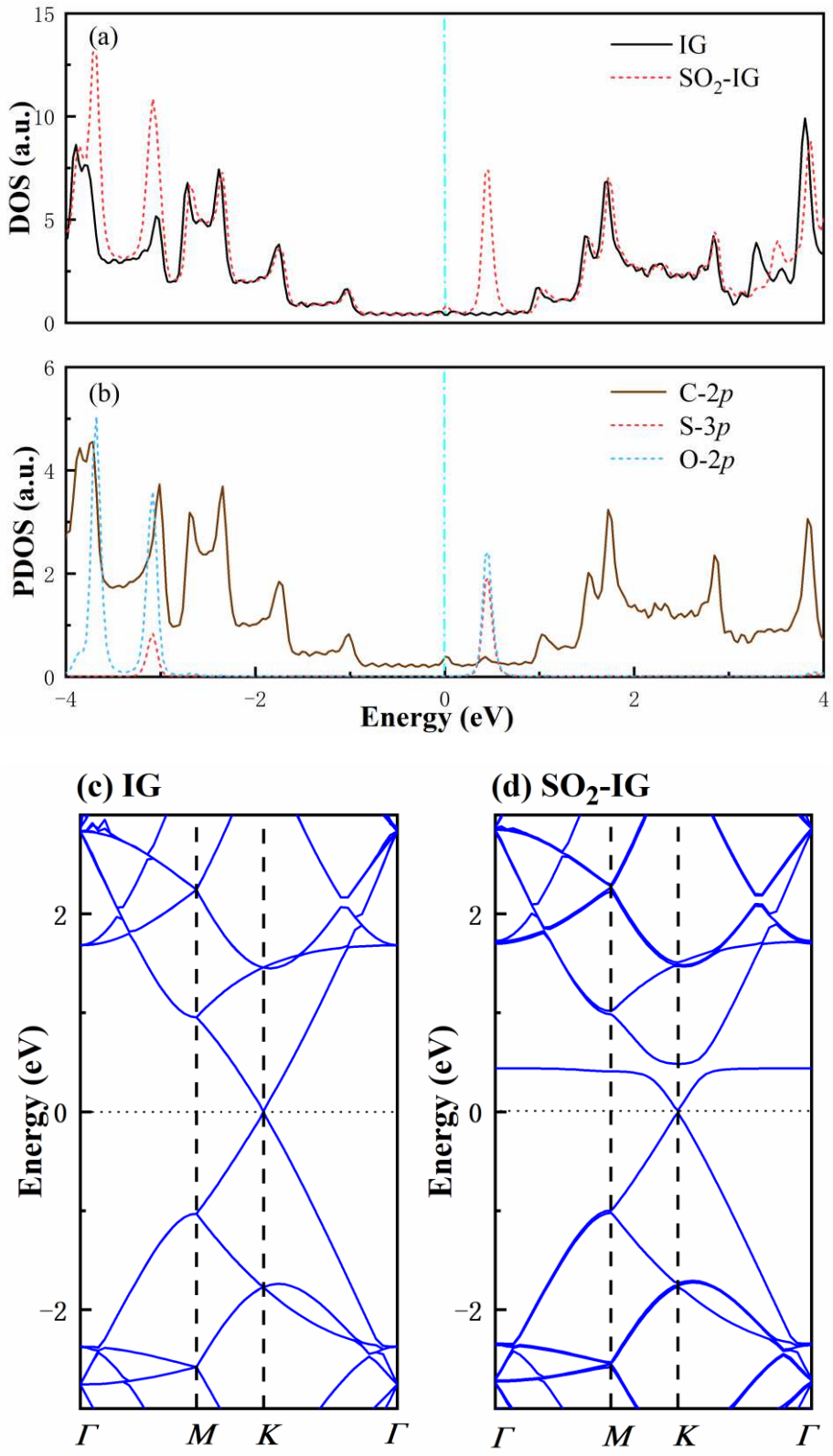

Fig. 4. DOS of IG with and without SO_2 molecule adsorption. The band structures for IG and SO_2 adsorbed on IG. The dotted line at zero indicates the Fermi level.

3.3 Adsorption performance of vacancy graphene layer

Studies have demonstrated that vacancy defects can enhance the gas sensitivity and adsorption stability of graphene [39, 40]. In this part, the adsorption performance of SO_2 molecule on VG is examined. **Fig. 2(b)** presents the most favorable state of SO_2 on VG. The optimal adsorption site is that an O atom of SO_2 molecule is close to the VG to form an O-C bond, which is consistent with previous researches [41]. After adsorption, as shown in **Table 1**, the VG adsorption system with the E_{ads} of 2.522 eV and the adsorption distance is 1.425 Å. The charge transfer is $0.325e$ from VG to SO_2 molecule, which is higher than that of IG adsorption system. Moreover, the VG has a magnetic moment of 1.7 μB in our calculations because of the loss of a C atom in VG, which can cause unpaired electrons to be generated around the defect, and then result in asymmetry in the spin-up and spin-down energy level, and thereby generate magnetism. After adsorbing SO_2 molecule, the substrate becomes non-magnetic. The adsorption of SO_2 molecule pair unpaired electrons with the electrons in SO_2, forming chemical adsorption. After the spin-up and spin-down electrons are coordinated, the formation of the bond orbital makes the magnetism disappear. The results suggest that mono-vacancy defect improves the adsorption activity of graphene for SO_2 molecules.

As presented in **Fig. 5(a)**, the DOS curve at the Fermi level changes significantly. Analysis of the electronic properties revealed that hybridization between the O-2p orbital and the C-2p orbital is existed, which is responsible for the enhancement of adsorption energy for SO_2-VG adsorption systems, as shown in **Fig. 5(b)**. Furthermore, the results of the band structures of VG showed that there is an energy band crossing

the Fermi level (see **Fig. 5(c)**), which is equivalent to a Fermi surface drop, similar to typical *p*-type doping. **Fig. 5(d)** shows the bands of the system of VG with SO_2 molecule. Removing a C atom result in the creation of unpaired electrons, leading to a local state. After adsorbing SO_2 molecule, the gas molecule hybridized with unpaired electrons to form stable bonding-antibonding orbitals, and the opening of band gap energy is 0.17 eV to form stable structures. According to the obtained results, it can be seen that VG can effectively interact with SO_2 molecule, and its electronic and transport properties are dramatically enhanced after exposure to this molecule. In addition, compared to the IG system, the existence of vacancy defect improved the adsorption stability with the higher adsorption energy and charge transfer. This means that the SO_2 molecule has strong adsorption capacity on graphene with a vacancy defect, which can be attributed to the broken π-band around the vacancy defect generating the unpaired electrons. In general, vacancy defect enhances the adsorption performance of graphene on SO_2 molecule.

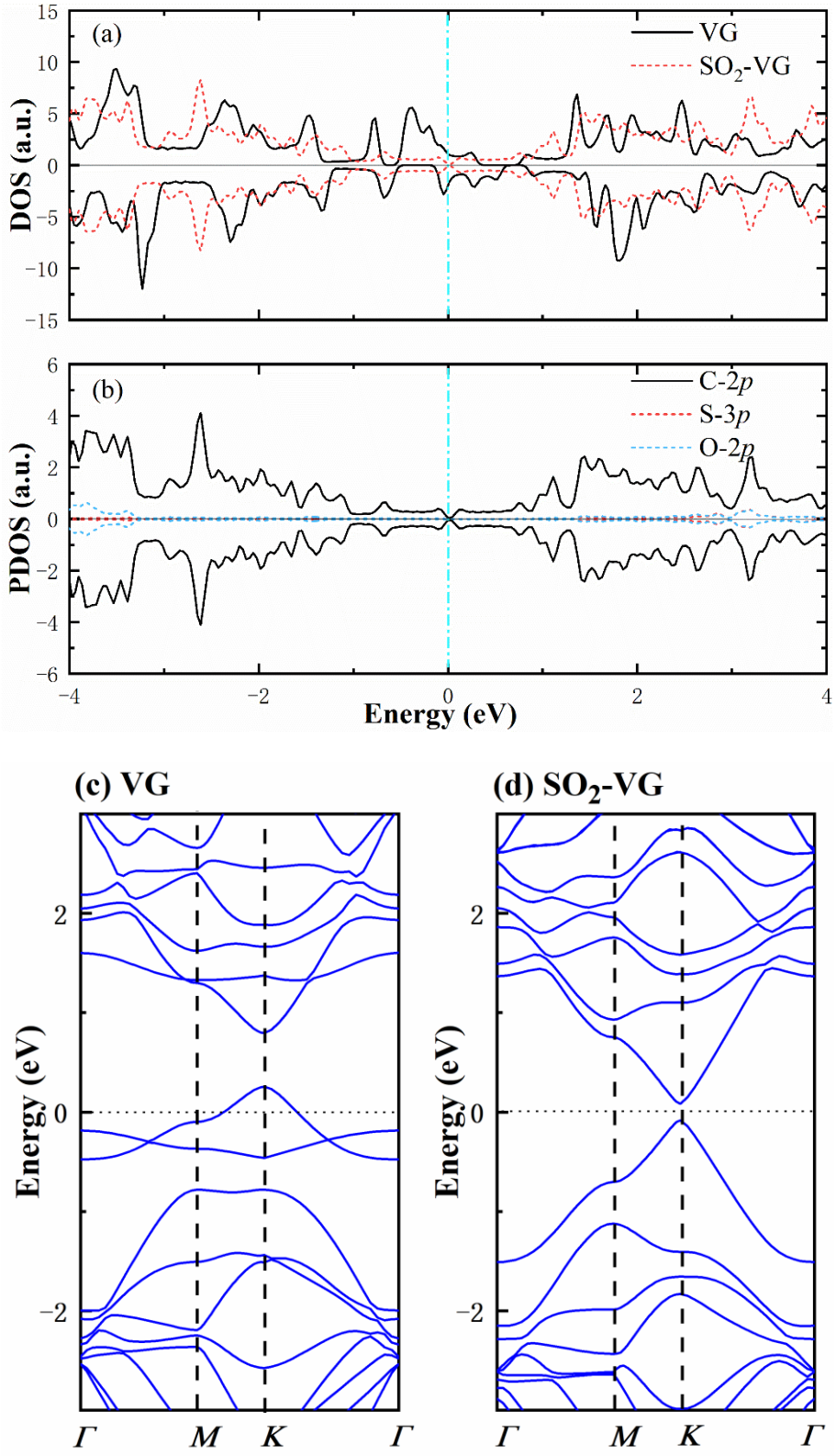

Fig. 5. The total density of states (DOS) of VG with and without SO_2 molecule adsorption. The band structure for VG and SO_2 adsorbed on VG. The dotted line at zero indicates the Fermi level.

3.4 Adsorption performance of Pd-doped graphene layer

In this part, we substituted a C atom on the surface of graphene with a Pd atom to achieve the PdG adsorption configuration. There are obvious differences between the relaxed IG and PdG in terms of geometric structure, lattice constant and bond length. This confirms that doping palladium and other impurities in graphene will cause 6MR deformation near the doping site due to different atomic radiation. The most stable configuration and various geometric parameters of the optimized PdG adsorption system are shown in **Fig. 2(c)** and **Table 1**. The E_{ads} of the SO_2-PdG system is 5.650 eV and the adsorption distance is 2.281 Å. The larger adsorption energy and shorter adsorption distance suggest that chemical adsorption between SO_2 and PdG is enhanced. Moreover, there is an obvious charge transfer between SO_2 and PdG, and the amount of charge transfer is $0.524e$. Compared with VG adsorption system, Pd-doping disrupts the original stable structure of pure graphene and enhances behavior for SO_2 adsorption. Besides, the enhancement is also demonstrated by the slight activation of the S-O bond in the SO_2 molecule after adsorption, which extends to 1.525 Å.

The DOS of PdG with and without adsorption of SO_2 molecule is depicted in **Fig. 6(a)**. It can be observed that PdG has two sharp peaks at the Fermi level after adsorbed SO_2 molecule, one of which crosses the Fermi level. In addition, the values of peaks surrounding -4 eV, -1 eV and 2 eV increase in varying degrees. As exhibited in **Fig. 6(b)**, the effective hybridization between the Pd-4*d* orbital and the O-2*p* orbital can be determined as their overlap in the atomic DOS, which confirms the chemical interaction between the SO_2 molecule and the adsorption substrate. **Fig. 6(c)** displays the band

structure of the system of PdG after achieving full relaxation. As a consequence of chemisorption, all the bands are dispersive and very similar to the case of IG (see **Fig. 4(a)**) expect that a Pd atom is added to cause the opening of an energy gap of value of about 0.24 eV. From **Fig. 6(d)**, it can be seen that the E_g is disappeared after the adsorption of SO_2 molecule. The reason is that during the formation of the Pd-C bond on PdG, Pd atom transfers electrons to the surrounding C atoms, causing the local C atoms to undergo electron hybridization and form distinct bonding and antibonding orbitals, thus opening the band gap. However, with the completion of adsorption, the electrons in the originally saturated Pd-C hybrid orbitals transfer to SO_2 molecule, resulting in a zero band gap. Meanwhile, it can be confirmed from **Fig. 6(a)** that there is a shark peak crossing the Fermi level after adsorption, which can be regarded as a conductor.

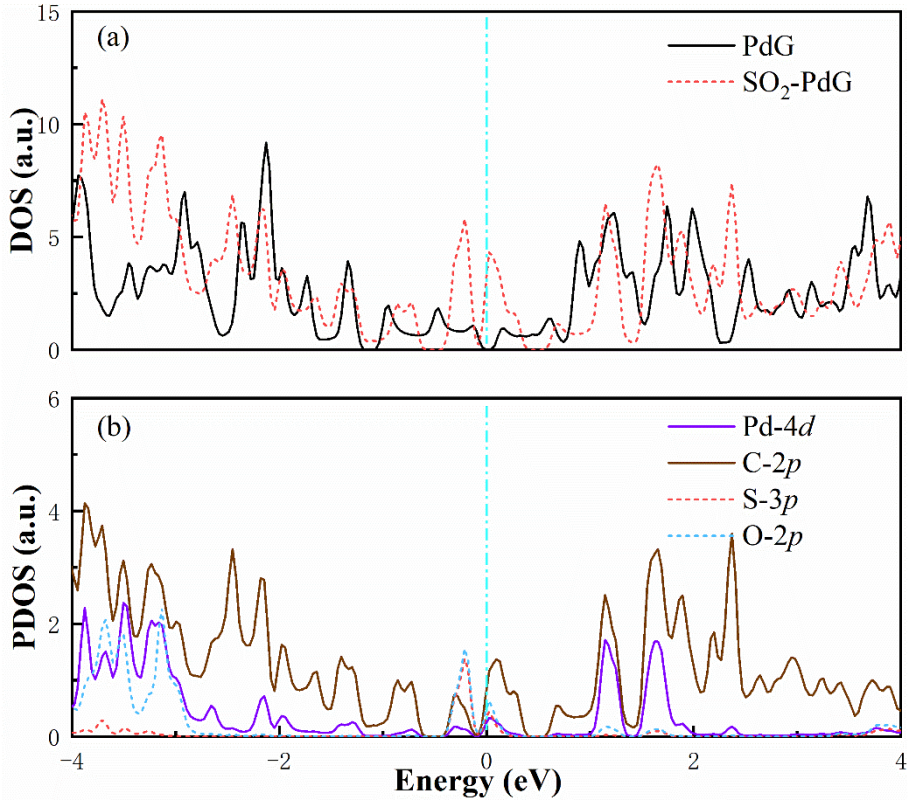

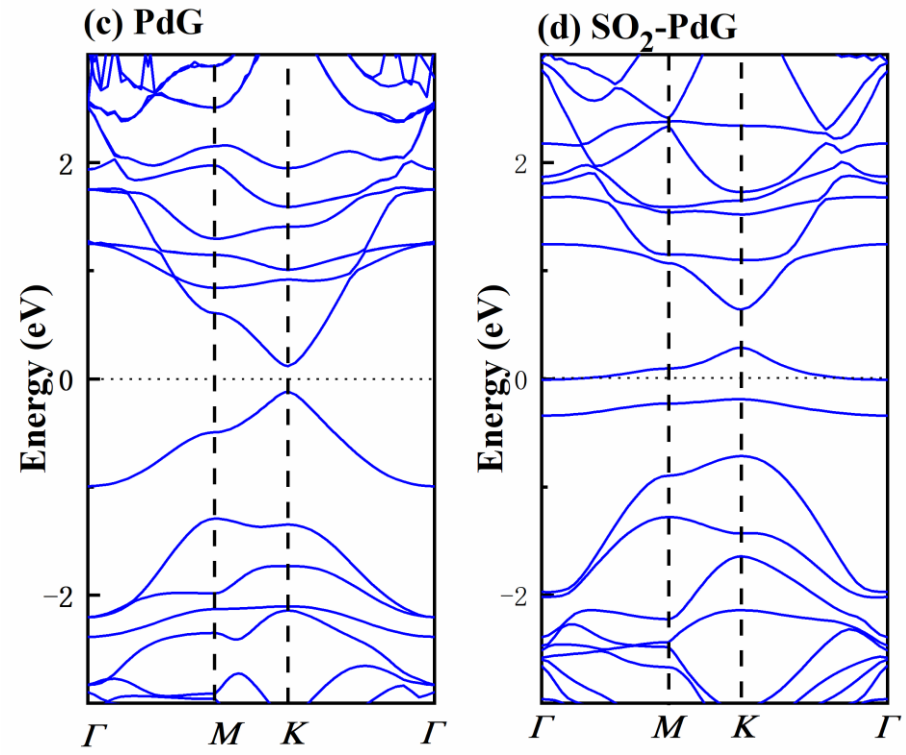

Fig. 6. The total density of states (DOS) of PdG with and without SO_2 molecule adsorption. The band structure for PdG and SO_2 adsorbed on PdG. The dotted line at zero indicates the Fermi level.

3.5 Adsorption performance of Pd-doped vacancy graphene layer

To investigate the adsorption mechanism of the defect-dopant combination, the adsorption behavior of the coexistence of vacancy defect and Pd dopant was discussed. After the complete relaxation of the structure, it is observed that Pd atom in vacancy defect tends to directly occupy the position of the rotation bond, which forms two five-ring and two six-ring structures. The structural parameters of Pd-VG sample are presented in **Fig. 1(d)**, and it shows the bond length from Pd to the nearest C atom is 2.026 Å. The C-C bond length of Pd-VG ranges from 1.392 Å to 1.395 Å. Pd atom protruding from the plane caused large deformities in the area around the defect, and

the structural properties of Pd-VG have changed considerably following optimization. The most favorable configuration is that an O atom of SO_2 points to the graphene plane by molecular relaxation, as shown in **Fig. 2(d)**. Versus the PdG adsorption system, the E_{ads} of SO_2-Pd-VG system is reduced to 0.734 eV. Meanwhile, the adsorption distance is slightly increased to 2.290 Å. These results show that the adsorption of SO_2 on Pd-VG is weaker than that on PdG. The tetra-coordination system (four Pd-C bonds) formed by Pd-VG structure tends to be stable, and the number of unpaired electrons within the system is reduced compared with the tri-coordination system of PdG, which leads to its weak adsorption capacity.

To further understand the electronic properties of the Pd-VG adsorption system, the DOS and band structures are depicted in **Fig. 7**. As can be seen from **Fig. 7(a)**, SO_2 adsorption causes changes in the electronic properties of Pd-VG, showing a sharp peak near the Fermi level, and the peaks around -4 eV, 2 eV and 3 eV also increase to varying degrees. In addition, Pd-4*d* and O-2*p* orbitals have overlapping peaks near -4 eV and 0 eV, which confirms the hybridization between orbitals, as shown in **Fig. 7(b)**. Consequently, Pd-VG may also detect SO_2 molecules based on the change in conductivity before and after adsorption. As can be seen from **Fig. 7(c)**, Pd-VG is semi-metallic and has a direct band gap of 0.5 eV. After adsorbing SO_2 molecule, the E_g (0.25 eV) was slightly decreased as shown in **Fig. 7(d)**. Moreover, a new local energy level appears at the top of the valence band, which can serve as a trapping center for atoms or molecules that IG and VG cannot capture. In this case, doping Pd atom forms new electronic holes, thereby enhancing the conductivity of graphene. It also proves

that Pd-VG is a typical *p*-type semiconductor. Based on the above analysis, it is concluded that heteroatom Pd introduces the localized state within E_g, which improves the reactivity of graphene.

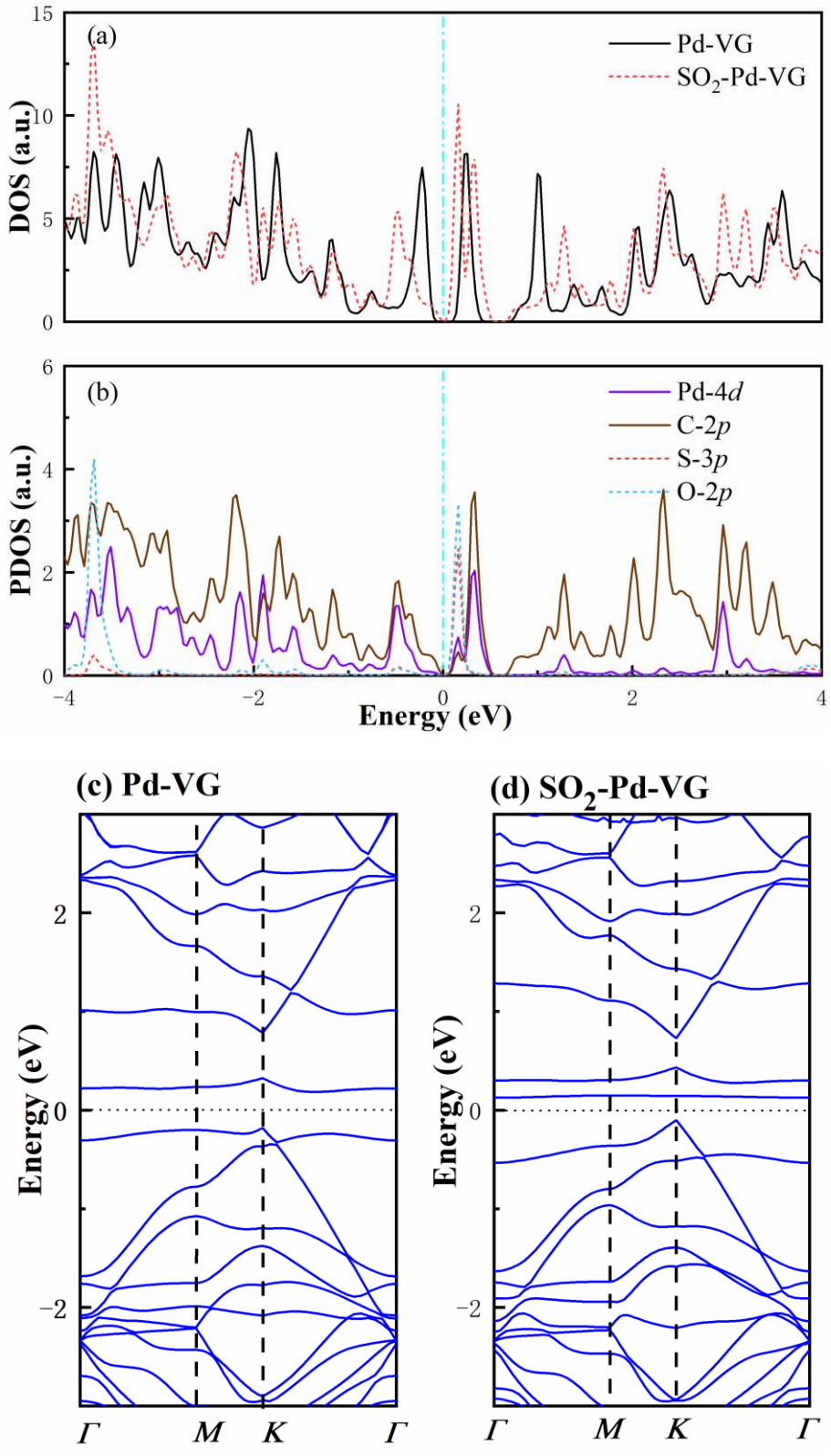

Fig. 7. The total density of states (DOS) of Pd-VG with and without SO_2 molecule adsorption. The band structure for Pd-VG and SO_2 adsorbed on Pd-VG. The dotted line at zero indicates the Fermi level.

4. Conclusions

Based on DFT calculations, the adsorption behavior of SO_2 gas molecule on IG, VG, PdG, and Pd-VG has been systematically studied and discussed. The adsorption mechanism is revealed from the perspectives of adsorption energy, adsorption distance, charge transfer, band structure, DOS and PDOS. The results show that SO_2 exhibits extremely weak interaction on IG, which is typical physical adsorption. On the other hand, doping Pd atom or introducing vacancy defect can significantly strengthen the interaction between SO_2 molecule and graphene substrate and the adsorption energy is approximately 19 times and 8 times from IG, respectively, exhibiting strong chemical adsorption. Consequently, the VG and PdG could be the ideal choices for SO_2 gas sensor. Furthermore, modifying graphene with Pd dopant and vacancy defect is beneficial for detecting SO_2 gas. However, the coexistence of the two methods results in a decrease in unmatched electrons and a significant reduction in the adsorption capacity of SO_2. Compared to PdG, the adsorption energy of Pd-VG is decreased by approximately 87%. However, due to its obvious electronic structure characteristics, Pd-VG may be used as a candidate material for detecting SO_2 gas molecules.

Funding

This research was funded by the Science and Technology Research Program of Chongqing Municipal Education Commission (KJQN201901108), the Scientific

Research Foundation of Chongqing University of Technology (2019ZD06, 2020ZDZ026), and the Postgraduate Innovation Program of Chongqing University of Technology (clgycx20202120).

Conflicts of interest

There are no conflicts to declare.

Availability of data and material

The data used to support the findings of this study are available from the corresponding author upon request.

Code availability

Vienna ab-initio simulation package program.

Authors' contributions

Yanjie Xu: Conceptualization, Methodology, Writing-Original draft preparation, Writing-Reviewing and Editing; Jiangling Tian, Lei Li: Investigation; Qingwei Zhang, Jun'an Zhang and Yunhua Lu: Supervision.

References

1. Meng Z, Stolz RM, Mendecki L, Mirica KA (2019) Electrically-Transduced Chemical Sensors Based on Two-Dimensional Nanomaterials. Chem Rev 119:478–598. https://doi.org/10.1021/acs.chemrev.8b00311

2. Lee E, VahidMohammadi A, Yoon YS, et al (2019) Two-Dimensional Vanadium Carbide MXene for Gas Sensors with Ultrahigh Sensitivity Toward Nonpolar Gases. ACS Sens 4:1603–1611. https://doi.org/10.1021/acssensors.9b00303

3. Meng F-L, Guo Z, Huang X-J (2015) Graphene-based hybrids for chemiresistive gas sensors. TrAC Trends in Analytical Chemistry 68:37–47. https://doi.org/10.1016/j.trac.2015.02.008

4. Liu X-Y, Zhang J-M, Xu K-W, Ji V (2014) Improving SO2 gas sensing properties of graphene by introducing dopant and defect: A first-principles study. Applied Surface Science 313:405–410. https://doi.org/10.1016/j.apsusc.2014.05.223

5. Li J, Pang L, He K, Zhang L (2019) Theoretical Study of the Gas Sensing Mechanism of N_3 &Ni Doped Double Vacancies Defect Graphene Upon SF_6 Decompositions. IEEE Access 7:145567–145573. https://doi.org/10.1109/ACCESS.2019.2945469

6. Zhou Q, Zeng W, Chen W, et al (2019) High sensitive and low-concentration sulfur dioxide (SO2) gas sensor application of heterostructure NiO-ZnO nanodisks. Sensors and Actuators B: Chemical 298:126870. https://doi.org/10.1016/j.snb.2019.126870

7. Kumar V, Roy DR (2019) Single-layer stanane as potential gas sensor for NO2, SO2, CO2 and NH3 under DFT investigation. Physica E: Low-dimensional Systems and Nanostructures 110:100–106. https://doi.org/10.1016/j.physe.2019.02.001

8. Lin W, Li F, Chen G, et al (2020) A study on the adsorptions of SO2 on pristine and phosphorus-doped silicon carbide nanotubes as potential gas sensors. Ceramics International 46:25171–25188. https://doi.org/10.1016/j.ceramint.2020.06.307

9. Hsueh T-J, Lu C-L (2019) A hybrid YSZ/SnO_2/MEMS SO_2 gas sensor. RSC Adv 9:27800–27806. https://doi.org/10.1039/C9RA03607E

10. Zheng Y, Manh TD, Nam ND, et al (2020) Optimization of micro Knudsen gas sensor for high precision detection of SO2 in natural gas. Results in Physics 16:102933. https://doi.org/10.1016/j.rinp.2020.102933

11. Song H-Q, Liu Z, Zhang D-B (2019) Interlayer vibration of twisted bilayer graphene: A first-principles study. Physics Letters A 383:2628–2632. https://doi.org/10.1016/j.physleta.2019.05.025

12. Kumar V, Vikrant K, Kim K-H (2019) Use of graphene-based structures as platforms for the trace-level detection of gaseous formaldehyde and insights into their superior sensing potentials. TrAC Trends in Analytical Chemistry 121:115694. https://doi.org/10.1016/j.trac.2019.115694

13. Bo Z, Guo X, Wei X, et al (2019) Density functional theory calculations of NO2 and H2S adsorption on the group 10 transition metal (Ni, Pd and Pt) decorated graphene. Physica E: Low-dimensional Systems and Nanostructures 109:156–163. https://doi.org/10.1016/j.physe.2019.01.012

14. Han C, Chen Z (2019) Adsorption properties of O2 on the unequal amounts of binary co-doped graphene by B/N and P/N: A density functional theory study. Applied Surface Science 471:445–454. https://doi.org/10.1016/j.apsusc.2018.12.019

15. Gao X, Zhou Q, Wang J, et al (2020) Performance of Intrinsic and Modified

Graphene for the Adsorption of H2S and CH4: A DFT Study. Nanomaterials 10:299. https://doi.org/10.3390/nano10020299

16. Schedin F, Geim AK, Morozov SV, et al (2007) Detection of individual gas molecules adsorbed on graphene. Nature Mater 6:652–655. https://doi.org/10.1038/nmat1967

17. Faye O, Raj A, Mittal V, Beye AC (2016) H2S adsorption on graphene in the presence of sulfur: A density functional theory study. Computational Materials Science 117:110–119. https://doi.org/10.1016/j.commatsci.2016.01.034

18. Yang S, Lei G, Xu H, et al (2019) A DFT study of CO adsorption on the pristine, defective, In-doped and Sb-doped graphene and the effect of applied electric field. Applied Surface Science 480:205–211. https://doi.org/10.1016/j.apsusc.2019.02.244

19. Huang S, Panes-Ruiz LA, Croy A, et al (2021) Highly sensitive room temperature ammonia gas sensor using pristine graphene: The role of biocompatible stabilizer. Carbon 173:262–270. https://doi.org/10.1016/j.carbon.2020.11.001

20. Tit N, Said K, Mahmoud NM, et al (2017) Ab-initio investigation of adsorption of CO and CO 2 molecules on graphene: Role of intrinsic defects on gas sensing. Applied Surface Science 394:219–230. https://doi.org/10.1016/j.apsusc.2016.10.052

21. Olsson E, Chai G, Dove M, Cai Q (2019) Adsorption and migration of alkali metals (Li, Na, and K) on pristine and defective graphene surfaces. Nanoscale 11:5274–5284. https://doi.org/10.1039/C8NR10383F

22. Yang S, Qian X, Xu H, et al (2021) The improved CO adsorption/sensing performance of Stone-Wales defected graphene doped with Fe: A DFT study. Physica E: Low-dimensional Systems and Nanostructures 128:114603. https://doi.org/10.1016/j.physe.2020.114603

23. Ghanbari R, Safaiee R, Sheikhi MH, et al (2019) Graphene Decorated with Silver Nanoparticles as a Low-Temperature Methane Gas Sensor. ACS Appl Mater Interfaces 11:21795–21806. https://doi.org/10.1021/acsami.9b00625

24. Srivastava S, Jain SK, Gupta G, et al (2020) Boron-doped few-layer graphene nanosheet gas sensor for enhanced ammonia sensing at room temperature. RSC Adv 10:1007–1014. https://doi.org/10.1039/C9RA08707A

25. Shukri MSM, Saimin MNS, Yaakob MK, et al (2019) Structural and electronic properties of CO and NO gas molecules on Pd-doped vacancy graphene: A first principles study. Applied Surface Science 494:817–828. https://doi.org/10.1016/j.apsusc.2019.07.238

26. Liang X-Y, Ding N, Ng S-P, Wu C-ML (2017) Adsorption of gas molecules on Ga-doped graphene and effect of applied electric field: A DFT study. Applied Surface Science 411:11–17. https://doi.org/10.1016/j.apsusc.2017.03.178

27. Capote Mastrapa G, Freire FL (2019) Plasma-Treated CVD Graphene Gas Sensor Performance in Environmental Condition: The Role of Defects on Sensitivity. Journal of Sensors 2019:1–7. https://doi.org/10.1155/2019/5492583

28. Li K, Li N, Yan N, et al (2020) Adsorption of small hydrocarbons on pristine, N-doped and vacancy graphene by DFT study. Applied Surface Science 515:146028. https://doi.org/10.1016/j.apsusc.2020.146028

29. Blöchl PE (1994) Projector augmented-wave method. Phys Rev B 50:17953–17979. https://doi.org/10.1103/PhysRevB.50.17953

30. Kresse G, Furthmüller J (1996) Efficiency of ab-initio total energy calculations for metals and semiconductors using a plane-wave basis set. Computational Materials Science 6:15–50. https://doi.org/10.1016/0927-0256(96)00008-0

31. Kresse G, Furthmüller J (1996) Efficient iterative schemes for ab initio total-energy calculations using a plane-wave basis set. Phys Rev B 54:11169–11186. https://doi.org/10.1103/PhysRevB.54.11169

32. Kresse G, Joubert D (1999) From ultrasoft pseudopotentials to the projector augmented-wave method. Phys Rev B 59:1758–1775. https://doi.org/10.1103/PhysRevB.59.1758

33. Perdew JP, Burke K, Ernzerhof M (1996) Generalized Gradient Approximation Made Simple. Phys Rev Lett 77:3865–3868. https://doi.org/10.1103/PhysRevLett.77.3865

34. Monkhorst HJ, Pack JD (1976) Special points for Brillouin-zone integrations. Phys Rev B 13:5188–5192. https://doi.org/10.1103/PhysRevB.13.5188

35. Blöchl PE, Jepsen O, Andersen OK (1994) Improved tetrahedron method for Brillouin-zone integrations. Phys Rev B 49:16223–16233. https://doi.org/10.1103/PhysRevB.49.16223

36. Harl J, Schimka L, Kresse G (2010) Assessing the quality of the random phase approximation for lattice constants and atomization energies of solids. Phys Rev B 81:115126. https://doi.org/10.1103/PhysRevB.81.115126

37. Yang D, Yang N, Ni J, et al (2017) First-principles approach to design and evaluation of graphene as methane sensors. Materials & Design 119:397–405. https://doi.org/10.1016/j.matdes.2017.01.087

38. Gaur V, Asthana R, Verma N (2006) Removal of SO2 by activated carbon fibers

in the presence of O2 and H2O. Carbon 44:46–60. https://doi.org/10.1016/j.carbon.2005.07.012

39. Wu X-J, Fei Z-J, Liu W-G, et al (2019) Adsorption and desorption of hydrogen on/from single-vacancy and double-vacancy graphenes. NUCL SCI TECH 30:69. https://doi.org/10.1007/s41365-019-0584-4

40. Jia X, Zhang H, Zhang Z, An L (2020) Effect of doping and vacancy defects on the adsorption of CO on graphene. Materials Chemistry and Physics 249:123114. https://doi.org/10.1016/j.matchemphys.2020.123114

41. Zhou Q, Ju W, Su X, et al (2017) Adsorption behavior of SO 2 on vacancy-defected graphene: A DFT study. Journal of Physics and Chemistry of Solids 109:40–45. https://doi.org/10.1016/j.jpcs.2017.05.007